

Alignment and orientation in the electron-impact excitation of the 2^1P state of He from 40 to 500 eV

N. C. Steph and D. E. Golden

Department of Physics and Astronomy, University of Oklahoma, Norman, Oklahoma 73019

(Received 14 November 1979)

Electron-photon angular correlations between electrons which have excited the 2^1P state of He and photons from the $2^1P \rightarrow 1^1S$ transition have been studied for 100-, 200-, and 500-eV incident electrons. Values of λ and $|\chi|$ obtained from these measurements are compared to values which have been obtained in other experiments and calculations. The results are in good agreement with the recent distorted-wave calculation of Madison. The values of λ and $|\chi|$ from all experiments have been combined to examine the behavior of the Fano-Macek alignment and orientation parameters for electron energies from 40 to 500 eV.

I. INTRODUCTION

Electron-photon angular correlation measurements were first reported by Eminyán *et al.* in 1973.¹ These measurements covered the energy range from 40 to 200 eV, but the range of electron scattering angles θ_e was restricted to $\theta_e > 15^\circ$ at all energies, and to $\theta_e \leq 25^\circ$ for energies > 80 eV. The only other measurements for energies above 80 eV were those of Ugbabe *et al.*² at 120 eV for values of θ_e of 10° and 16° . A summary of the other measurements for energies ≤ 80 eV may be found in Steph and Golden.³

The results of such angular correlation measurements are usually expressed in terms of the parameters λ and $|\chi|$ which describe the excited state. For excitation of the 2^1P state from the 1^1S ground state, the excited-state wave function is given by

$$\psi(2^1P) = a_0 |10\rangle + a_1 |11\rangle + a_{-1} |1-1\rangle, \quad (1)$$

where the complex excitation amplitudes a_{M_L} describe the excitation of the different magnetic sublevels. Since the scattering process has mirror symmetry in the scattering plane, $a_1 = -a_{-1}$, and the total differential cross section is given by

$$\sigma = |a_0|^2 + 2|a_1|^2. \quad (2)$$

The parameter $|\chi|$ is the absolute value of the phase difference between the complex scattering amplitudes a_0 and a_1 and

$$\lambda = |a_0|^2 / \sigma. \quad (3)$$

The dimensionless parameters λ and $|\chi|$ are functions of the electron energy E and the electron scattering angle θ_e . They describe the excited state of the atom after undergoing a collision and (together with σ) provide a complete determination of the excitation amplitudes. The approximations used in a calculation can give insight into the relative importance

of various effects, such as exchange, in the scattering process provided the calculation predicts the correct values of λ , $|\chi|$, and σ . Thus it is important to obtain accurate values of these quantities.

For an excitation at a given E and θ_e , the angular distribution of deexciting radiation in the scattering plane is given in terms of λ and χ as

$$f(\lambda, \chi, \theta_\gamma) = \lambda \sin^2 \theta_\gamma + (1 - \lambda) \cos^2 \theta_\gamma - [\lambda(1 - \lambda)]^{1/2} \cos \chi \sin 2\theta_\gamma, \quad (4)$$

where θ_γ is the angle of photon emission. Although the 2^1P-1^1S photons result from an electric dipole transition, studying electron-photon angular correlations leads to a knowledge of the electric quadrupole and magnetic dipole distributions for the excited state. The excited-state population has been described by Fano and Macek⁴ in terms of an orientation vector \vec{O} and an alignment tensor \underline{A} in order to separate the geometrical and dynamical effects. For 1^1S-2^1P excitation in helium by electron impact, \vec{O} has one nonvanishing component which is proportional to the average value of the net angular momentum of the excited state and is related to λ and χ by

$$O_1^{z01} = \langle L_y \rangle / [L(L+1)] = -[\lambda(1-\lambda)]^{1/2} \sin \chi. \quad (5)$$

The alignment tensor has three nonvanishing components:

$$\begin{aligned} A_0^{z01} &= \langle 3L_x^2 - L^2 \rangle / [L(L+1)] = (1-3\lambda)/2, \\ A_{1+}^{z01} &= \langle L_x L_z + L_z L_x \rangle / [L(L+1)] \\ &= [\lambda(1-\lambda)]^{1/2} \cos \chi, \\ A_{2+}^{z01} &= \langle L_x^2 - L_z^2 \rangle / [L(L+1)] = (\lambda-1)/2. \end{aligned} \quad (6)$$

It should be noted that O_1^{z01} and A_{1+}^{z01} are not independent and that A_0^{z01} and A_{2+}^{z01} are not independent. The third independent parameter in this formulation is the monopole moment, which is propor-

tional to σ .⁵

It has been shown by Blum and Kleinpoppen⁵ that the induced magnetic moment of the excited atom is determined by the orientation vector and that the electric quadrupole tensor is proportional to the alignment tensor, while all higher multipoles vanish. The orientation vector is directly given by the transfer of angular momentum to the atom, and its behavior as E and θ_e are varied can give physical insight into the scattering process. The alignment tensor specifies the distribution of the electronic charge in the atom and this, in turn, specifies the anisotropy of the emitted radiation. Therefore Eq. (4) may be rewritten as

$$f(\lambda, \chi, \theta_\gamma) = \frac{2}{3} + \frac{1}{3} A_0^{\text{co}1} (3 \cos^2 \theta_\gamma - 1) - A_{1+} \sin 2\theta_\gamma + A_{2+} \sin^2 \theta_\gamma. \quad (7)$$

Equation (7) may be rewritten in terms of the associated Legendre function, $P_l^m(\cos \theta_\gamma)$,

$$f(\lambda, \chi, \theta_\gamma) = \frac{2}{3} [1 + A_0^{\text{co}1} P_0^2(\cos \theta_\gamma) - A_{1+}^{\text{co}1} P_2^1(\cos \theta_\gamma) + \frac{1}{2} A_{2+}^{\text{co}1} P_2^2(\cos \theta_\gamma)]. \quad (8)$$

The first term in Eq. (8) represents the monopole contribution to the radiation distribution. The remaining terms represent contributions to the radiation distribution from linear quadrupoles in the scattering plane along the z axis, at 45° to the z axis, and at 90° to the z axis, respectively. The nonvanishing components of \underline{A} are coefficients which determine the intensity of radiation with a given angular distribution.

The simplest theory which makes clear predictions of λ and χ is the first Born approximation (FBA). The results of the FBA depend only on the kinematics of the collision. Accordingly, no angular momentum may be transferred to the atom along the direction of linear-momentum transfer \vec{K} . Thus, along the K axis there is a $\Delta M_L = 0$ selection rule. This implies that there will be no radiation emitted along the direction of \vec{K} . This means that $\chi = 0$ independent of E and θ_e . The FBA predicts that $\lambda = \cos^2 \theta_K$ where θ_K is the angle between \vec{K} and the incident electron beam. Because of the nature of this approximation, one might at first expect this prediction to be valid for small scattering angles and high energies. However, while the FBA prediction for λ is in reasonable agreement with the results of Eminyan *et al.*¹ at 50 eV, the agreement becomes worse as the energy increases. The FBA places emphasis on the role played by the direction of linear-momentum transfer \vec{K} . The angle θ_K in the FBA corresponds to the angle where the angular distribution of radiation is a minimum, θ_{min} . This prediction is in much better agreement with the data of Eminyan *et al.*,¹ even where the FBA

predictions for λ and χ are in very poor agreement. The value of θ_{min} may be expressed in terms of λ and χ as

$$\tan 2\theta_{\text{min}} = 2[\lambda(1-\lambda)]^{1/2} \cos \chi / (2\lambda - 1). \quad (9)$$

So it is clear that if the FBA correctly predicts θ_{min} when χ is not zero, then its prediction of λ must be incorrect.

Another fairly simple approximation which in general has a broader range of applicability than the FBA, is the Glauber approximation. (The Glauber approximation satisfies the optical theorem in contrast to the FBA in which the scattering amplitudes are purely real.) However, it was pointed out by Eminyan *et al.*¹ that the Glauber approximation, despite some success in predicting differential cross sections, predicts that λ and χ are both independent of E and θ_e . Therefore we must turn to more elaborate theoretical calculations.

The various theoretical calculations prior to 1978⁶⁻¹⁰ have been reviewed by Bransden and McDowell.¹¹ A meaningful comparison of the various calculations is difficult because they differ in the nature of the approximations and within a given approximation they may differ in the choice of atomic potentials and wave functions. For example, the recent distorted-wave calculation of Baluja and McDowell¹² gives very different results than the distorted-wave calculation of Madison.¹³ The only significant difference between these two calculations is the choice of atomic wave functions. Baluja and McDowell used a simple analytic form while Madison used numerical Hartree-Fock orbitals. If these two calculations had used the same wave functions, they would in principle have given the same results.

The only calculation in reasonable agreement with all of the results of Eminyan *et al.*¹ for $E \geq 100$ eV, is the distorted-wave calculation of Madison.¹³ However, this calculation gives values of $|\chi|$ about 20% larger than those measured by Eminyan *et al.*¹ The distorted-wave calculation of Bransden and Winters⁸ using the second-order potential method gives the best agreement for $|\chi|$ but it is in very poor agreement with the results for λ . It should be noted that the calculation of Bransden and Winters⁸ neglects final-state distortion which should be an important consideration.

In a recent publication, Steph and Golden³ have reported electron-photon angular correlation measurements in electron-helium collisions for 2^1P excitation at an incident electron energy of 80 eV. In this paper we present further angular correlation measurements for 2^1P excitation of helium at electron energies of 100, 200, and 500

eV. In addition, we have combined the data of Sutcliffe *et al.*¹⁴ with that of Steph and Golden³ to give results for the full angular range from 5° to 100° and 155° at 80 eV. And finally, we combine all of the present results with the results of the other experiments^{1,2} at all energies to examine the behavior of the Fano-Macek⁴ alignment and orientation parameters as a function of energy.

II. THE EXPERIMENT

The theory of electron-photon angular correlations first given by Macek and Jaecks¹⁵ has since been fully discussed by several authors.^{1,5} The experimental apparatus and procedures used in the present work are identical to those described by Steph and Golden³ and will only be briefly discussed here. The experimental geometry is shown in Fig. 1. The electron beam is incident along the z axis and intersects the atomic beam which is incident along the y axis. (This choice of axes is referred to as the collision frame.) The scattered electrons are energy analyzed by a hemispherical electron-energy analyzer which is tuned to pass electrons which have lost 21.22 eV. A channel electron multiplier is used to detect the transmitted electrons. The overall resolution of the system is independent of the incident electron energy and is 0.40 eV. The xz plane is the scattering plane. The electron detector may be rotated in the range $-5^\circ \leq \theta_e \leq 150^\circ$. The photons emitted by the excited helium atoms are detected by a suitably housed channel electron multiplier whose axis is also in the scattering plane. The angular position of the photon detector θ_γ may be varied in the range $50^\circ \leq \theta_\gamma \leq 145^\circ$. A Faraday cup is provided to collect the unscattered electron beam. The electron-beam current is typically 1 μ A and the background pressure with the target-gas beam on is $\sim 3 \times 10^{-7}$ Torr. The pressure in the helium beam has been estimated to be $\sim 3 \times 10^{-5}$ Torr.

The pulses from the electron detector are used to start a time-to-amplitude converter (TAC), and suitably delayed pulses from the photon de-

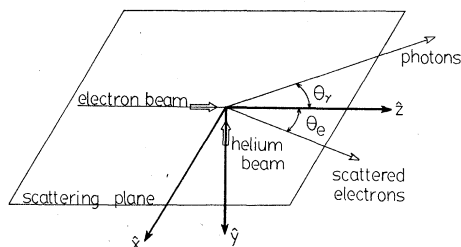


FIG. 1. The geometry of the experiment in the collision frame.

tor are used to stop the TAC. The output of the TAC is fed into a multichannel analyzer operated in the pulse-height analysis mode in order to generate the time spectrum of coincidence events. Electrons and photons from the same scattering event arrive with a definite time correlation. When counted for a time T these true coincidences form a peak on a background of accidental coincidences due to electrons and photons from different scattering events. For fixed values of θ_e and E , the number of true coincidences N_c will vary with θ_γ according to Eq. (4).

Measurements of N_c at several values of θ_γ are analyzed using the method of least squares to extract optimum values of λ and $|\chi|$. This procedure is discussed in Steph and Golden³ and involves solving the equations which minimize the χ^2 analytically. This solution yields the optimum values of λ and $|\chi|$ and enables the development of analytic expressions for the statistical uncertainties in λ and $|\chi|$. Prior to analysis, the data must be corrected for the systematic effects of the finite solid angle of the photon detector and for scattering from the background helium. In addition, one must ensure that resonant trapping of the photons is not significant. These points have been fully discussed in Steph and Golden.³

The cross section σ decreases as the electron energy is increased from 80 eV. In addition, σ decreases sharply for increasing values of θ_e at all values of E . The decreasing rate of scattered electrons at large values of E and θ_e leads to increasing counting times. When the scattered electron rate falls to $\sim 20 \text{ sec}^{-1}$, the rate of accidental coincidences falls to $\sim 0.2 \text{ sec}^{-1}$ and the rate of true coincidences is less than 1% of the accidental rate. Thus, coincidences must be counted for as long as one week at each value of θ_γ in order to reduce statistical uncertainty to an acceptable level. In this work, no measurements were made for values of θ_e where the scattered electron rate was $\leq 20 \text{ sec}^{-1}$.

III. RESULTS

The present experimental results are tabulated in Table I where the values of λ and $|\chi|$ and their uncertainties are listed as a function of energy and electron scattering angle. We also list the values of θ_{\min} calculated from Eq. (8) and the results of the FBA and the distorted-wave calculation of Madison¹³ (MDW) for λ , $|\chi|$, and θ_{\min} . The experimental values of λ at 80 eV were obtained by combining the results obtained in the present apparatus by Steph and Golden³ with those obtained by Sutcliffe *et al.*¹⁴ in an earlier version of the apparatus. The values of Sutcliffe *et al.*¹⁴ were normalized to the 10° result of the calculation of

TABLE I. Experimental results and comparison with theory. (The distorted-wave calculations of Madison is denoted by MDW and the first Born approximation is denoted by FBA.)

Energy (eV)	θ_e (deg)	λ			χ (rad)		θ_{\min} (deg)		
		Expt. ^a	Theory MDW	Theory FBA	Expt. ^a	Theory ^b MDW	Expt. ^a	Theory MDW	Theory FBA
80 ^c	5	0.749 ± 0.015	0.761	0.79	0.231 ± 0.220	0.259	29.7 ± 1.0	28.8	27.3
	10	0.488 ± 0.015	0.470	0.52	0.370 ± 0.038	0.425	44.3 ± 1.0	43.1	43.9
	20	0.305 ± 0.012	0.306	0.31	0.568 ± 0.054	0.905	58.3 ± 1.0	62.1	56.2
	30	0.445 ± 0.023	0.413	0.27	1.182 ± 0.053	1.304	53.1 ± 1.5	61.9	58.7
	40	0.642 ± 0.060	0.651	0.28	(1.60) ^d	1.527	-2.8 ± 15.0	3.9	58.1
	50	0.913 ± 0.048	0.860	0.32	1.994 ± 0.146	1.666	-7.8 ± 3.2	-2.6	55.6
	60	0.950 ± 0.062	0.965	0.37	2.424 ± 0.416	1.948	-10.0 ± 6.6	-4.1	52.5
	70	0.927 ± 0.140	0.990	0.44	(3.0) ^d	3.075	-15.5 ± 12.3	-5.7	48.4
	80	0.861 ± 0.120	0.968	0.50	2.570 ± 0.402	2.260	-19.4 ± 7.2	-6.7	45.0
	90	0.894 ± 0.079	0.925	0.58	2.001 ± 0.243	1.944	-9.0 ± 5.5	-6.4	40.4
	100	0.838 ± 0.108	0.885	0.65	1.842 ± 0.175	1.738	-8.1 ± 5.5	-3.9	36.3
155	0.920 ± 0.150	0.962	0.96		1.082		5.5	11.5	
100	5	0.67 ± 0.03	0.660	0.69	0.25 ± 0.18	0.243	34.8 ± 1.0	35.4	33.8
	10	0.36 ± 0.01	0.365	0.40	0.40 ± 0.04	0.456	53.8 ± 1.0	53.7	50.8
	16	0.28 ± 0.01	0.267	0.27	0.52 ± 0.03	0.778	59.7 ± 1.0	63.2	58.7
	30	0.49 ± 0.03	0.447	0.21	1.40 ± 0.05	1.318	48.4 ± 2.7	56.5	62.7
	40	0.76 ± 0.05	0.736	0.24	1.70 ± 0.12	1.455	-6.0 ± 5.4	6.1	60.7
200	5	0.34 ± 0.014	0.318	0.33	0.25 ± 0.07	0.260	54.6 ± 1.0	56.0	54.9
	10	0.20 ± 0.010	0.161	0.15	0.43 ± 0.06	0.601	64.8 ± 1.0	69.1	67.2
	20	0.19 ± 0.022	0.245	0.11	0.95 ± 0.12	1.082	71.8 ± 2.5	70.8	70.6
	30	0.64 ± 0.031	0.627	0.13	1.31 ± 0.14	1.160	20.7 ± 7.5	28.3	68.9
	40	0.95 ± 0.050	0.925	0.17	1.00 ± 0.20	0.760	7.3 ± 4.2	12.1	65.7
500	5	0.19 ± 0.02		0.08	0.29 ± 0.20		64.8 ± 1.5		73.6
	10	0.09 ± 0.01		0.04	0.58 ± 0.17		74.9 ± 1.6		78.5
	15	0.14 ± 0.02		0.05	0.70 ± 0.20		71.8 ± 2.5		77.8

^aUncertainties quoted for λ and χ represent one standard deviation.

^bThe FBA predicts $\chi=0$ for all E and θ_e .

^cThe experimental values of λ and their uncertainties at 80 eV are the combined results of Refs. 3 and 14 as discussed in the text.

^dThese values of χ are interpolated as discussed in the text.

Madison and Calhoun,⁹ $\lambda=0.479$. We have re-normalized their values to the 10° result of Steph and Golden,³ $\lambda=0.488$. Although this renormalization results in only ~2% change in the values of λ , it frees the data from dependence on a particular calculation. The two sets of data are combined by taking the average of their values weighted by their uncertainties. The values of $|\chi|$ listed for $\theta_e=40^\circ$ and 70° at 80 eV are based on a smooth interpolation of the results of Steph and Golden³ for $|\chi|$ as a function of θ_e . An additional criterion used was that the interpolated values of $|\chi|$ combined with the measured values of λ yielded values of θ_{\min} , O_{i-}^{c01} , and A_{i+}^{c01} which were also consistent with the smooth interpolation of the results of Steph and Golden³ for these quantities. Figure 2 shows the data for λ and $|\chi|$ for 100, 200, and 500 eV plotted as a function of θ_e . We have also plotted the previous results of Eminyay *et al.*¹ at 100 and 200 eV along with the results of three distorted-wave (DW) calcula-

tions.^{8,10,13} At each energy we have measured one point in common with Eminyay *et al.*¹ and these results all agree within one standard deviation. The three DW calculations differ in their choice of wave functions and potentials. The calculation of Madison,¹³ which is the only DW calculation that includes distortion of the final state, is in good agreement with the present results for λ . The agreement is also fairly good for $|\chi|$ except for the small range of angles from 15° to 25° where the calculation of Madison¹³ gives larger values of $|\chi|$ at all energies. The calculation of Bransden and Winters⁸ is in fairly good agreement with the present results for $|\chi|$ but it is in very poor agreement with the results for λ . In contrast, the results of Scott and McDowell¹⁰ are in fair agreement with the results for λ , at least at 200 eV, but they are in very poor agreement with the results for $|\chi|$. The results of these three calculations indicate that further refinement of the wave functions and potentials in the

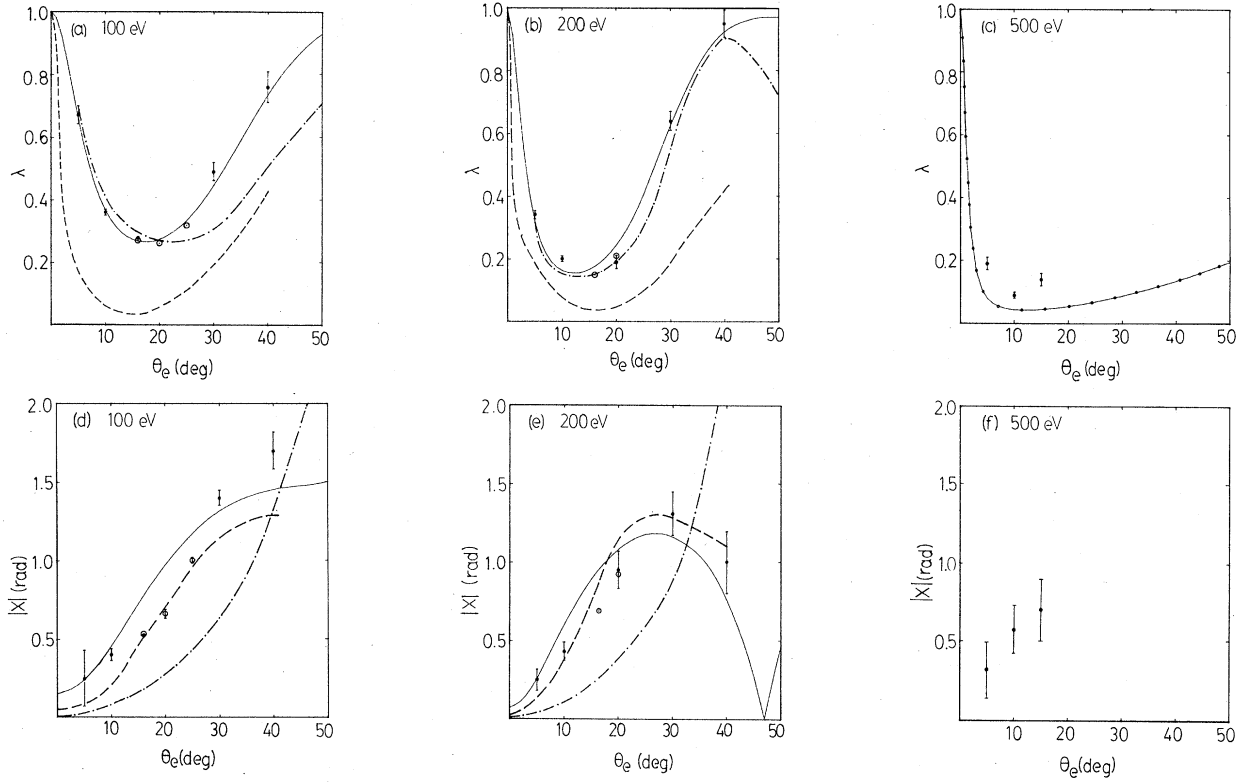


FIG. 2. The variation of λ with electron scattering angle at different electron energies: (a) 100 eV, (b) 200 eV, and (c) 500 eV. The variation of $|\chi|$ with electron scattering angle at different electron energies: (d) 100 eV, (e) 200 eV, and (f) 500 eV. ●, present work; ○, results of Ref. 1; —, calculation of Ref. 13; ---, calculation of Ref. 8; - · -, calculation of Ref. 10; ○—, FBA.

distorted-wave theory should yield very good agreement with experimental results.

The FBA for λ is in reasonable agreement with the results for λ , $\theta_e \leq 20^\circ$, at 100 eV (see Table I). At 200 eV this agreement is only good for $\theta_e \leq 5^\circ$. The FBA does not agree with any of the data for λ at 500 eV which can be seen in Fig. 2. Thus, as the energy is increased, the FBA is in increasingly poorer agreement with experimental results. This is in contrast to the FBA prediction for σ which is in better agreement with experiment at higher energies. This fact, along with the prediction that χ is zero for all energies, is sufficient to conclude that the FBA is inadequate to describe the excitation process in detail. However, it should be noted that the FBA prediction for θ_{\min} is in good agreement with the data for $\theta_e \leq 20^\circ$ for $E \leq 200$ eV, and is in good agreement with the present results at 500 eV, at least for $\theta_e \leq 15^\circ$. Thus the importance that the FBA places on the direction of linear-momentum transfer for the excitation process seems to be well founded for small scattering angles. It is clear however that the $\Delta M_L = 0$ selection rule along the K axis is not correct.

IV. DISCUSSION OF RESULTS AND CONCLUSIONS

The behavior of λ and χ as a function of θ_e and E has been discussed. These parameters may be combined to form the alignment and orientation parameters which can then be used to describe the multipole moments of the excited state. Since these quantities are more closely related to the structure and anisotropy of the excited atom, we will consider the behavior of \bar{O} and \bar{A} in some detail.

The nonvanishing component of the orientation vector O_{1-1}^{001} is directly related to the dynamics of the excitation process. Equation (5) shows that O_{1-1}^{001} is directly proportional to the expectation value of angular momentum transferred to the atom perpendicular to the scattering plane. Indeed, since $L = 1$, we may write

$$\langle L_y \rangle = 2O_{1-1}^{001}. \quad (10)$$

Further, we know that $L_y = M_L \hbar$ so that the average $\langle L_y \rangle$ varies between -1 and $+1$. This reflects the fact that the atom is in a coherent mixture of states and does not generally possess a definite M_L value. We may rewrite Eq. (1) as

$$\psi(2^1P) = |a_0| \psi_z + \sqrt{2} |a_1| e^{i\chi} \psi_x, \quad (11)$$

where $\psi_z = |10\rangle$ and $\psi_x = (1/\sqrt{2})(|11\rangle - |1-1\rangle)$. Thus, when $\lambda=1$ the atom is in the pure state ψ_z , and L_y vanishes so that $\langle L_y \rangle$ also vanishes. When $\lambda=0$ the atom is in the pure state ψ_x , and L_y may be ± 1 with equal probability so that $\langle L_y \rangle$ again vanishes. Thus, the nonvanishing values of O_{1-1}^{e01} may only occur when the atom is in a coherent mixture of ψ_x and ψ_z , and there is interference between the complex scattering amplitudes a_0 and a_1 . The maximum value of O_{1-1}^{e01} is realized when $|a_0| = 2|a_1|$ (i.e., $\lambda=0.5$), and $\chi = \pi/2$. When $\chi=0$ or is an integral multiple of π , O_{1-1}^{e01} vanishes. When the value of χ passes through 0 or $\pm\pi$, the sign of O_{1-1}^{e01} changes. The experiment only measures the principal value of χ . Thus, values of χ reported are in the range $0 \leq \chi \leq \pi$. However, theory suggests that χ does pass through $-\pi$ at 80 and 100 eV, and through 0° at 200 eV.^{10,12,13} Restricting the discussion to 80 eV, and considering only the theory of Madison,¹³ χ is negative in the range $0^\circ \leq \theta_e \leq 180^\circ$ and passes through $-\pi$ at $\theta_e \approx 70^\circ$. Thus, O_{1-1}^{e01} is positive for $\theta_e \leq 70^\circ$ and negative for $\theta_e > 70^\circ$.

In order to relate the behavior of O_{1-1}^{e01} to the collision process we shall look at the collision semiclassically. When an electron is scattered to a given angle, θ_e , the scattering may take either of the two principal paths shown in Fig. 3. In Fig. 3(a), the electron approaches the He atom with a negative impact parameter and scatters from the attractive polarizability potential to a positive scattering angle. In order to conserve angular momentum, the atom in Fig. 3(a) must obtain positive angular momentum perpendicular to the scattering plane; i.e., L_y must lie along the positive y axis. So, referring to Eq. (5), this implies that O_{1-1}^{e01} is positive for this collision. In Fig. 3(b) the electron must be incident with a

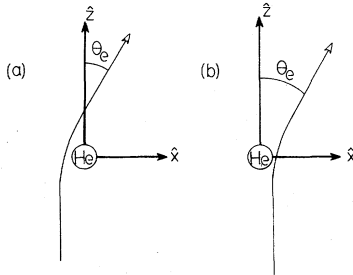


FIG. 3. The two principal paths for semiclassical scattering of electrons from helium. (a) The electron is incident with a negative impact parameter and scatters from the attractive polarizability potential to the positive angle, θ_e . (b) The electron is incident with a positive impact parameter and scatters from the repulsive potential of the He electrons to the same positive angle, θ_e .

positive impact parameter if it is to scatter from the repulsive potential of the helium electrons and reach a positive scattering angle. In order to conserve angular momentum in this case, the atom must obtain negative angular momentum which implies that O_{1-1}^{e01} is negative. Using this semiclassical model, we may explain the behavior of O_{1-1}^{e01} as follows: When the electron is scattered to $\theta_e = 0^\circ$, there can be no change in the angular momentum of the atom perpendicular to the scattering plane. Therefore O_{1-1}^{e01} vanishes at $\theta_e = 0^\circ$. As the scattering angle increases from 0° , the amount of angular momentum transferred to the atom perpendicular to the scattering plane, L_y , increases. Since the dominant scattering potential for small angles is the long-range attractive potential due to atomic polarizability, L_y is positive. Thus, O_{1-1}^{e01} is positive and increases towards its extremal value of 0.5. However, as the scattering angle continues to increase, the impact parameter decreases and scattering from the repulsive potential of the helium electrons begins to become significant. Since the sign of the angular-momentum transfer due to repulsive scattering is opposite to that for attractive scattering, these processes compete and the value of O_{1-1}^{e01} may or may not reach the value of 0.5 before it decreases with θ_e . Then at some value of θ_e where the contributions from the two types of scattering are equal in magnitude, O_{1-1}^{e01} vanishes. As θ_e increases from this angle, the repulsive scattering becomes dominant and O_{1-1}^{e01} becomes negative and decreases to another extremum. As θ_e increases further, the transfer of angular momentum perpendicular to the scattering plane again decreases until at $\theta_e = 180^\circ$, O_{1-1}^{e01} vanishes.

The experimental results for $|O_{1-1}^{e01}|$ at 80 eV are plotted in Fig. 4 along with the results of calculations by Madison¹³ and Fon *et al.*¹⁶ The experimental results are generally in good agreement with the semiclassical description given above and with the calculation of Madison¹³ for $\theta_e \leq 70^\circ$ at 80 eV. Despite some disagreement in the range from 15° to 25° , the experimental results show an extremal value of $|O_{1-1}^{e01}| \approx 0.5$ at $\theta_e \sim 35^\circ$, and show that O_{1-1}^{e01} vanishes at $\theta_e \sim 70^\circ$. The second extremum is much broader than the extremum at $\theta_e \sim 35^\circ$, which indicates that there is little change in the relative importance of the two types of scattering in the backward direction. Using the results of Madison,¹³ $[O_{1-1}^{e01}(\theta_e = 110^\circ) \approx 0.35]$ the ratio of repulsive scattering to attractive scattering has a maximum value of ~ 3 . For $\theta_e > 70^\circ$, there are two sets of measurements that disagree. The results of Steph and Golden³ are in agreement with the calculation of Madison.¹³ The calculation of Fon *et al.*¹⁶ lies roughly half-

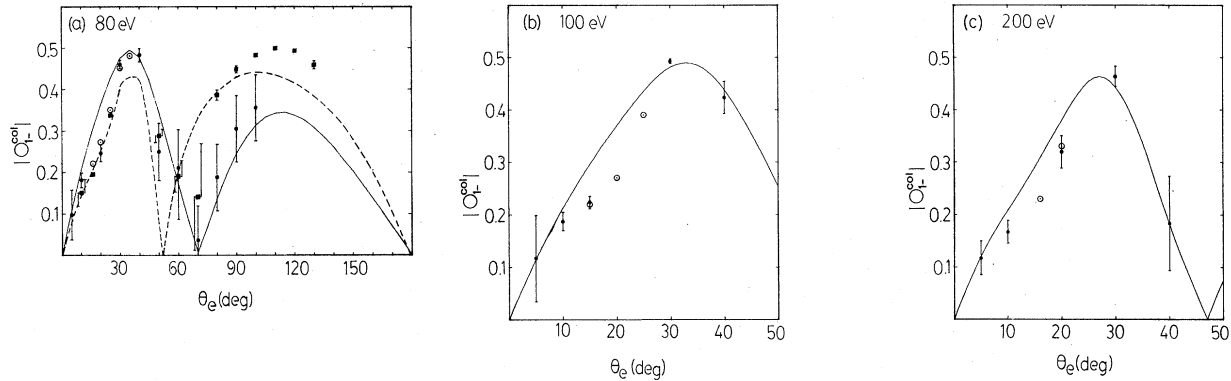


FIG. 4. The variation of $|O_{l=1}^{e01}|$ with electron scattering angle at different electron energies: (a) 80 eV, (b) 100 eV, and (c) 200 eV. \bullet , present work; \circ , results of Ref. 1; \blacksquare , results of Ref. 17; —, calculation of Ref. 13; ---, calculation of Ref. 16.

way between these results and the results of Hollywood *et al.*¹⁷ which predict that $|O_{l=1}^{e01}|$ reaches its maximum value of 0.5 at $\theta_e \sim 110^\circ$. So, the results of Hollywood *et al.*¹⁷ would indicate that repulsive scattering is virtually the only process for back scattering, while the two calculations and the results of Steph and Golden³ indicate that repulsive and attractive scattering are competing processes with repulsive scattering dominant by a maximum of a factor of 3 or 4.

We have discussed the disagreement between the two sets of experimental results for λ and $|\chi|$ in Steph and Golden³ where we argued that the experimental technique discussed by Hollywood *et al.*¹⁷ could impose systematic error on their data in the direction of the observed disagreement. It is also difficult to see how the attractive potential scattering could become completely insignificant for back scattering at 80 eV, although this would certainly be true at much larger energies as we discuss below. In any case, our semiclassical model is in qualitative agreement with the experimental results.

The behavior of $O_{l=1}^{e01}$ as the electron energy is increased may also be explained in our semiclassical model. As E increases, the velocity of the electron increases and the electron spends less time in the long-range field of the attractive potential. However, the influence of the repulsive potential is not significantly affected by increasing electron velocity. Thus, as E increases, the first extremum of $O_{l=1}^{e01}$ should occur at smaller values of θ_e and $O_{l=1}^{e01}$ should no longer reach its maximum value of -0.5 at the first extremum. In addition, the angular position of the zero crossing of $O_{l=1}^{e01}$ should decrease from 70° . The angular position of the second extremum should decrease from 110° and the value of $O_{l=1}^{e01}$ at this extremum should decrease toward its minimum value of -0.5 as energy increases and repulsive scat-

tering becomes more dominant. This is precisely the behavior seen by the experimental results at 100 and 200 eV for $\theta_e \leq 40^\circ$ shown in Fig. 4. The calculation of Madison is generally in good agreement with the present results in this energy range and also predicts the behavior of $O_{l=1}^{e01}$ for $\theta_e \geq 40^\circ$ discussed above.

The orientation at fixed scattering angles as a function of energy is shown in Fig. 5. The experimental points at fixed angles are joined by straight lines for clarity. The results show that for $\theta_e \leq 20^\circ$, $|O_{l=1}^{e01}|$ is virtually unaffected by increasing energy. Within our semiclassical model, this indicates that small-angle scattering is due solely to scattering from the long-range polarizability potential. The results also show that as energy increases, the position of the first extremum moves to smaller angles.

The nonvanishing components of the alignment tensor (A_0^{e01} , A_1^{e01} , and A_2^{e01}) are related to the average values of quadratic expressions in the angular-momentum vector and its components. Thus it is more difficult to visualize the physical process that they represent. However, we may

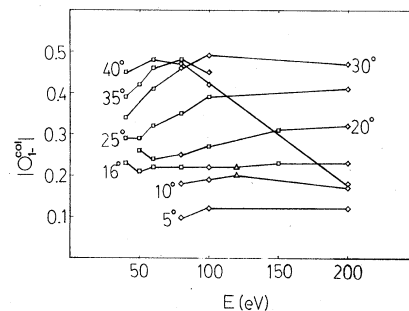


FIG. 5. The variation of $|O_{l=1}^{e01}|$ with electron energy at different scattering angles. \diamond , present results; \square , results of Ref. 1; \triangle , results of Ref. 2.

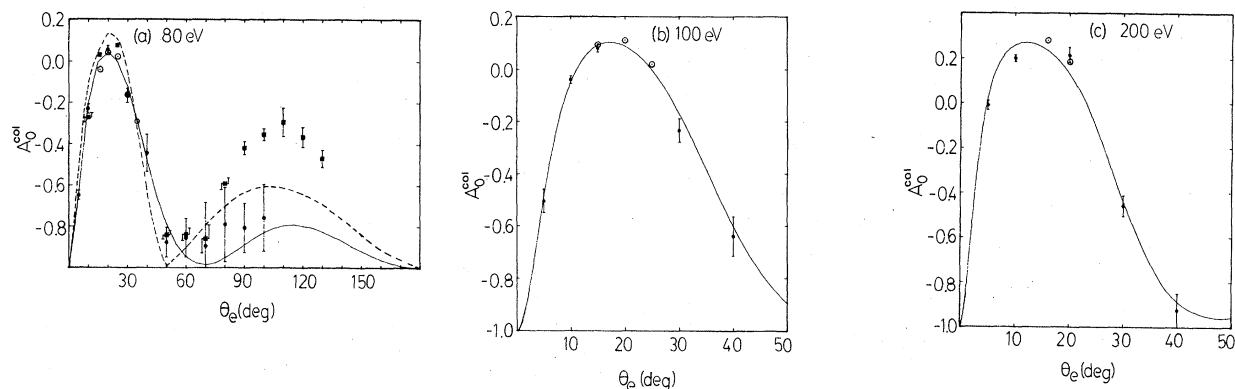


FIG. 6. The variation of A_0^{01} with electron scattering angle at different electron energies: (a) 80 eV, (b) 100 eV, and (c) 200 eV. The symbols are the same as Fig. 4.

note some marked similarities between the components of \underline{A} and \underline{O} . It is clear from Eqs. (5) and (6) that the behavior of O_1^{01} and A_1^{01} will be similar. The two remaining components of \underline{A} are also not independent, so we need only consider one of them. In Fig. 6 we show the data and calculations for A_0^{01} at 80, 100, and 200 eV. The qualitative behavior of A_0^{01} is strikingly similar to that of O_1^{01} . At 80 eV, there is a narrow extremum at about 30° and a broad extremum at about 110° . Between these extrema, at 70° , A_0^{01} returns to the value it had at $\theta_e = 0^\circ$. As the

energy is increased, the small-angle extremum occurs at decreasing values of θ_e and the size of the extremum decreases. The similarities in the qualitative behavior of \underline{O} and \underline{A} imply that the interplay between long-range attractive potential scattering and repulsive potential scattering is responsible for the observed variations.

ACKNOWLEDGMENTS

This work was supported in part by grants from the National Science Foundation and the U. S. Air Force Office of Scientific Research.

¹M. Eminyan, K. B. MacAdam, J. Slevin, and H. Kleinpoppen, Phys. Rev. Lett. **31**, 576 (1973); J. Phys. B **7**, 1519 (1974).

²A. Ugbabe, H. Arriola, P. J. O. Teubner, and E. Weigold, J. Phys. B **10**, 72 (1977).

³N. C. Steph and D. E. Golden, Phys. Rev. A **21**, 759 (1980).

⁴U. Fano and J. H. Macek, Rev. Mod. Phys. **45**, 553 (1973).

⁵K. Blum and H. Kleinpoppen, Phys. Rev. **52**, 203 (1979).

⁶C. J. Joachain and R. Vanderpoorten, J. Phys. B **7**, L528 (1974).

⁷M. R. Flannery and K. J. McCann, J. Phys. B **8**, 1716 (1975).

⁸B. H. Bransden and K. H. Winters, J. Phys. B **9**, 1115 (1976).

⁹D. H. Madison and R. V. Calhoun (unpublished).

¹⁰T. Scott and M. R. C. McDowell, J. Phys. B **9**, 2235 (1976).

¹¹B. H. Bransden and M. R. C. Dowell, Phys. Rep. **30**, 207 (1977); **46**, 250 (1978).

¹²K. L. Baluja and M. R. C. McDowell, J. Phys. B **12**, 835 (1979).

¹³D. H. Madison, J. Phys. B **12**, 3399 (1979).

¹⁴V. C. Sutcliffe, G. N. Haddad, N. C. Steph, and D. E. Golden, Phys. Rev. A **17**, 100 (1978).

¹⁵J. H. Macek and D. H. Jaecks, Phys. Rev. A **4**, 2288 (1971).

¹⁶W. C. Fon, K. A. Berrington, and A. E. Kingston, J. Phys. B **12**, L171 (1979).

¹⁷M. T. Hollywood, A. Crowe, and J. F. Williams, J. Phys. B **12**, 819 (1979).